Fragmentation cross sections of relativistic $^{84}_{36}$Kr and $^{109}_{47}$Ag nuclei in targets from hydrogen to lead

B. S. Nilsen,[1,*] C. J. Waddington,[1] J. R. Cummings,[3] T. L. Garrard,[3] and J. Klarmann[2]
[1]*School of Physics and Astronomy, University of Minnesota, Minneapolis, Minnesota 55455*
[2]*Department of Physics and the McDonnell Center for the Space Sciences, Washington University, St. Louis, Missouri 63130*
[3]*George W. Downs Laboratory, California Institute of Technology, Pasadena, California 91125*
(Received 2 June 1995)

With the addition of krypton and silver projectiles we have extended our previous studies of the fragmentation of heavy relativistic nuclei in targets ranging in mass from hydrogen to lead. These projectiles were studied at a number of discrete energies between 450 and 1500*A* MeV. The total and partial charge-changing cross sections were determined for each energy, target, and projectile, and the values compared with previous predictions. A new parametrization of the dependence of the total charge-changing cross sections on the target and projectile is introduced, based on nuclear charge radii derived from electron scattering. We have also parametrized the energy dependence of the total cross sections over the range of energies studied. New parameters were found for a previous representation of the partial charge-changing cross sections in hydrogen and a new parametrization has been introduced for the nonhydrogen targets. The evidence that limiting fragmentation has been attained for these relatively light projectile nuclei at Bevalac energies is shown to be inconclusive, and further measurements at higher energies will be needed to address this question.

PACS number(s): 25.75.+r, 25.70.Mn

I. INTRODUCTION

Studies of the interaction and fragmentation of relativistic nuclei interacting with target nuclei can provide insight into some aspects of nuclear structure. In addition, in order to study the origin and composition of the nuclei in the cosmic radiation, it is necessary to have accurate values of the cross sections describing the production of fragments by heavier nuclei interacting in the interstellar medium and, to a lesser degree, in the material of detectors. The source abundances of the cosmic ray nuclei deduced from local observations are critically dependent on the precision of the assumed cross sections. The sensitivity of calculations of propagation to the cross sections has been estimated for these ultraheavy cosmic ray nuclei by Clinton and Waddington [1]. Changes of as little as 10% in the assumed values of the cross sections can lead to 20% changes in the abundances that would be observed locally after propagation. Such changes are much greater than those produced by any reasonable changes in the assumed escape lengths from the confinement region. This is due principally to the short mean free paths for interactions of these heavy nuclei and their consequent insensitivity to escape.

Only since relativistic heavy ion accelerators have become available has it been possible to measure directly the inclusive production cross sections for elements in such interactions. Earlier the production cross sections in hydrogen could be determined only for certain individual radioactive isotopes produced by proton bombardment of target nuclei, while those in heavier targets could not be determined at all. The elemental and isotopic cross sections in hydrogen were then estimated by semiempirical extrapolations from the measurements. In principle, it is possible to measure directly all the elemental, and, with more difficulty, the isotopic cross sections required for calculations of the propagation of cosmic ray nuclei in any medium. However, it is impractical to undertake an experimental program to cover the entire spread of projectile and target masses over the wide range of energies needed. Therefore, it has been necessary to attempt to construct parametrizations of the dependence of the cross sections on the various variables that define them, using the experimentally determined values.

This paper reports the results from another in a series of experiments designed to study the fragmentation of relativistic heavy projectile nuclei interacting in a number of different targets. Both the total and inclusive partial charge-changing cross sections for the production of heavy fragments were measured. In previous publications [2–8] we have reported results for many different beams of projectiles, interacting in different targets (see Table I). In the work reported here, we have extended these studies to the fragmentation of projectiles of krypton, $^{84}_{36}$Kr, with incident energies of 1502*A*, 1198*A*, and 700*A* MeV, and projectiles of silver, $^{109}_{47}$Ag, with 1452*A*, 1212*A*, 1001*A*, 612*A*, and 504*A*

TABLE I. Previous experiments.

Projectile type	Projectile energy (*A* MeV)	Target type	Reference
$_{26}$Fe	1593	C,Al,Cu,Pb	[5,6]
$_{36}$Kr	1489	Al	[2,8]
$_{54}$Xe	1236	CH_2,C,Al	[2,8]
$_{57}$La	1214,1130,956,828,675,543	CH_2,C,Al,Cu	[5,6]
$_{67}$Ho	1128,976,822,648	CH_2,C,Al,Cu	[2–6,8]
$_{79}$Au	979,968,821,723,618	CH_2,C,Al,Cu	[2,3,5,6,8]

*Present address: Department of Physics and Astronomy, Louisiana State University, Baton Rouge, LA 70803.

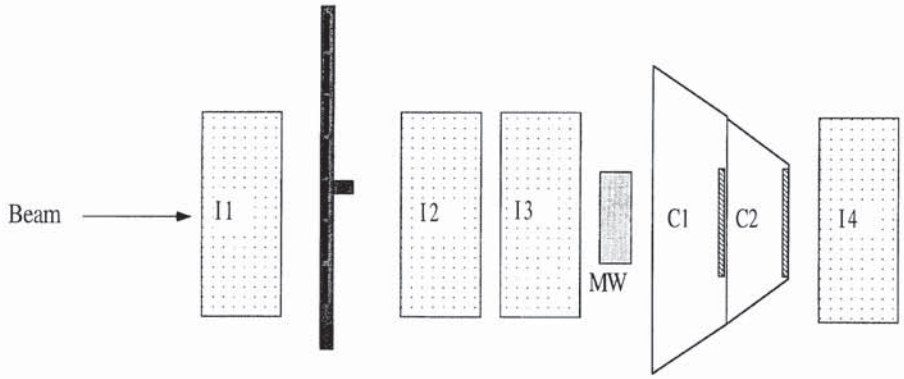

FIG. 1. HEAO Bevalac detector set up showing the relative position of the detectors used in this analysis. $I1$, $I2$, $I3$, and $I4$ are ion chambers. $C1$ and $C2$ are Cherenkov detectors. MW is a multiwire proportional chamber. The target changer is placed between $I1$ and $I2$. The array is 2.3 m long.

MeV. We have extended the range of targets in which these projectiles interacted to include tin, lead, and for the silver beam, lithium, in an attempt to achieve a better understanding of the physics involved.

The total cross sections $\sigma(P,T,K)$ have been measured for charge-changing interactions of projectile P (charge Z_P) in target T at a kinetic energy per nucleon K. The partial charge-changing cross sections $\sigma_{\Delta Z}(P,T,K,\Delta Z)$, with $\Delta Z=Z_f-Z_P$, have also been measured, for the production of heavy fragments of charge Z_f, for charge changes from $\Delta Z=+1$ to a minimum of $\Delta Z=-33$. These measurements have been compared to predictions from various parametrizations and models and, when combined with our earlier results, have been used to define a new parametrization for the negative charge changes. The production of fragments with charge pickup ($Z_f=Z_P+1$), which is relatively minor and represents a rather different phenomenon from charge loss, has been reported in Nilsen *et al.* [9].

II. DETECTOR ARRAY

We exposed an improved array of detectors consisting of ion chambers and Cherenkov detectors (Fig. 1), similar to those used previously [2–8] at the Beam 40 spectrometer facility at the Lawrence Berkeley Laboratories Bevalac. The active elements of this array consisted of four parallel plate ion chambers ($I1-I4$), two Cherenkov detectors with Pilot 425 radiators ($C1$ and $C2$), and a multiwire (MW) proportional chamber. The multiwire proportional chamber was used to center and focus the beam and thus to assure that the beam and fragments fell within the acceptance of the array, as well as to correct a small positional dependence in the Cherenkov detectors. Additional elements were included behind this array for detector development tests. A detailed description of this array and the individual detectors has been given by Nilsen [10]. This array was designed to determine both the charge of the incoming projectile and the charge of the heavy fast fragments emitted from an interaction in the target.

The signals from these detectors are proportional to the sum of squares of the charges Z_i of all the particles passing through them at one time, $Z_{\text{eff}}^2=\Sigma Z_i^2$. As long as the heaviest fragment produced in an interaction has a charge that is at least 0.4 of the projectile charge, it can be assumed that this sum will be dominated by the most highly charged fragment. This assumption is justified by the observation of well defined charge peaks for such fragments as shown in Fig. 2.

Data were taken whenever a signal in the first ion chamber was above background, as determined prior to the experiment. Background signals typically had amplitudes less than

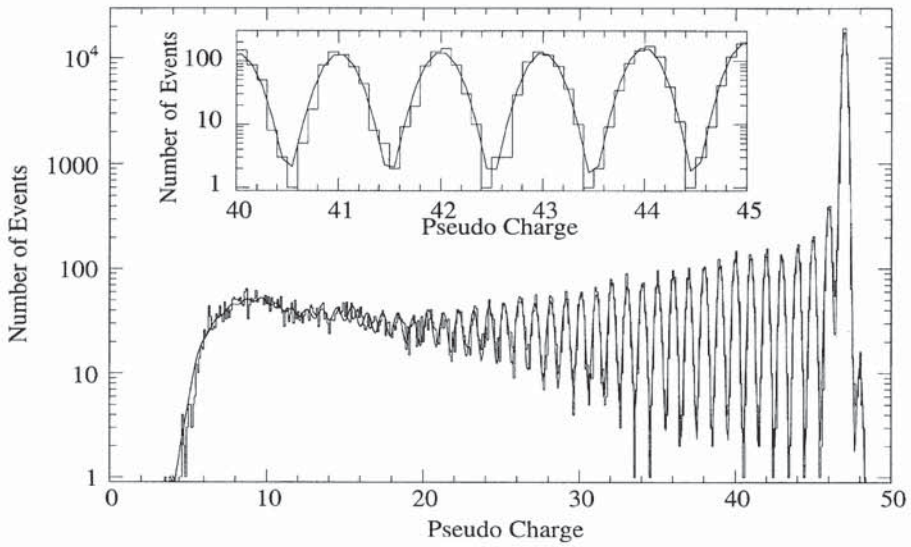

FIG. 2. Measured pseudocharge distribution of 1452A MeV Ag on a lithium target. The inset shows a blowup for small charge changes, with Gaussian fits to guide the eye and to indicate the degree of overlap between charge peaks.

TABLE II. Average interaction energy and energy loss in targets, ΔE, in A MeV, with total cross sections $\sigma(P,T,K)$ for charge-change in mb, with statistical and systematic uncertainties.

Energy	ΔE	$\sigma(H)$	Energy	ΔE	$\sigma(CH_2)$	Energy	ΔE	σ(Li)	Energy	ΔE	σ(C)
Kr											
1473		864±28±27	1473	24	1202±13±12				1442	85	1878±27±24
1168		768±28±30	1168	25	1094±9±6				1136	89	1746±26±29
666		764±26±14	666	29	1105±10±4				628	103	1788±24±13
Ag											
1419		1047±32±38	1419	20	1422±12±16	1409	40	2067±29±195	1388	81	2173±30±34
1178		1012±36±11	1178	21	1410±13±6	1168	42	2032±31±189	1147	84	2208±33±10
966		1045±30±13	966	22	1387±10±9	955	43	2017±30±183	933	87	2070±22±9
465		924±40±21	465	17	1335±15±10	454	39	1995±31±213	449	50	2076±37±18
Energy	ΔE	σ(Al)	Energy	ΔE	σ(Cu)	Energy	ΔE	σ(Sn)	Energy	ΔE	σ(Pb)
Kr											
1437	95	2410±40±60	1441	87	3231±74±89	1439	91	4150±109±166	1439	91	5067±162±132
1131	99	2160±34±19	1135	90	2948±58±53	1133	93	3603±79±49	1133	93	3713±112± 90
622	115	2241±34±21	628	104	3020±60±80	627	106	3855±88±155	627	106	4594±126±109
Ag											
1385	88	2728±39±84	1386	86	3679±66±100	1389	80	4598±124±167	1376	106	5767±134±165
1143	91	2719±43±26	1144	88	3841±73±59						
929	94	2646±39±37	931	92	3619±60±95	934	84	4584±90±82	921	111	5369±103±71
446	55	2869±59±48	444	61	3843±97±52	448	53	5032±175±117			

1% of the beam signals. The detector array had an acceptance, at $C2$, of ±68 mrad from the beam axis, which corresponds to a pseudorapidity of 3.38. This wide acceptance was designed to preclude the precise beam shape or tune having any influence on the measurement of cross sections. Nuclear emulsion measurements of emission angles of fragments have shown [11] that the heavy fragments typically have rather small transverse momenta. Scaling these results to the interactions studied here indicates that such a wide acceptance was sufficient to ensure that all the fast heavy fragments would be detected. The charge resolution achieved varied slightly from run to run but as a typical example, that of 1452A MeV silver ions after passing through a carbon target was 0.15 charge units (cu), entirely adequate to resolve individual elements.

For each projectile and for each energy, data were taken both with and without a target, in order to establish background corrections (target-in and target-out runs). Lacking a pure hydrogen target, the hydrogen cross sections were derived from a comparison of the cross sections measured in polyethylene (CH_2) and carbon [see Eq. (2)]. The thicknesses of the targets represented a compromise between a high event rate and a large correction for secondary interactions and energy losses. They were chosen to be less than about 20% of an interaction length and such that the energy loss in them did not exceed 100A MeV.

The mean energies in the targets are listed in Table II. For the three lowest incident energy beams, 700A MeV Kr and the 612A and 504A MeV Ag, the target-out runs were made at appropriately lower energies 599A, 554A, and 454A MeV, respectively, to better match the energy of the projectiles in the middle of the targets. We verified, by means of comparison of several sample runs, that there were no significant variations in the calculated cross sections with beam tune or during a run. For example, for one Ag run, two sets of target data were taken at different times with no significant differences in the resulting cross sections, which have therefore been combined in this analysis. The one exception to this was provided by another of the Ag runs, when the tune resulted in a beam that was so dispersed that reliable total cross sections could not be calculated: see Sec. IV A.

III. ANALYSIS

To assure a clean beam, projectile nuclei were accepted only if their signals in $I1$ were within four standard deviations (s.d.) of the beam peak for each run. This selection defined the number of entering particles, N_0.

The signals from each detector were calibrated using the known charges and velocities of the beam particles. Charge scales were established using the well-separated individual charge peaks of the fragments. The charge resolution for fragments was improved by using the signals from more than one detector. When the detectors were of the same type, with similar resolution, their signals were added together. By combining the signals from the ion chambers with those from the Cherenkov detectors, a pseudocharge was defined for each event. The different response of the Cherenkov and ion chambers can be seen, for the particular case of low energy Kr on a C target, in Fig. 3. The pseudocharge was derived using a coordinate transformation [10] involving the dependence of the signals in the Cherenkov detectors with radiators of refractive index n, $C \propto Z^2(1-1/n^2\beta^2)$, and ion chambers, $L \propto Z^2/\beta^2$, for charged particles with reduced velocity β. A histogram of the pseudocharges, for the example of high energy Ag on a Li target, is shown in Fig. 2. A particular fragment is assigned a charge Z_f if its pseudo-

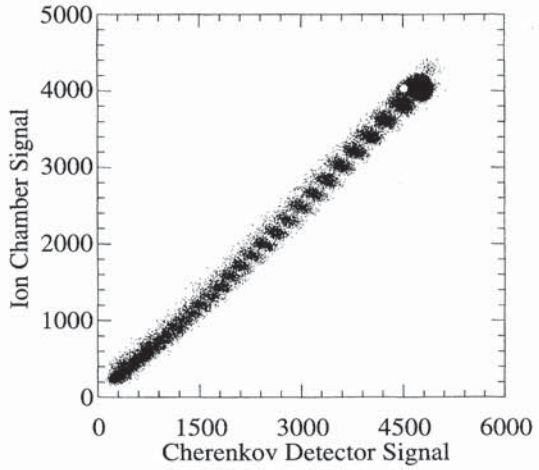

FIG. 3. Ion chamber signal vs Cherenkov detector signal with interaction cut applied for 700*A* MeV Kr on a carbon target. The circle of missing data near the beam peak is the result of the removal of particles that interacted in the Cherenkov detectors, but whose signals did not change enough to be removed by the other selections.

charge is within ± 0.5 cu of that fragment peak. An exception was made for events near the beam peak where, because of the magnitude of this peak, it was necessary to make the selections at -0.61 and $+0.75$ cu from the beam charge. These values were determined by locating the minima between the beam peak and its two neighbors at $\Delta Z = +1$ and -1.

To calculate the partial charge-changing cross sections, corrections had to be made for those nuclei that interacted in the detectors. The Cherenkov detectors are the thickest detectors in the array, being approximately 10% of an interaction length each, in contrast to the ion chambers with only 0.5% of an interaction length each. The Cherenkov detectors $C1$ and $C2$ were used for charge determinations due to their greater intrinsic resolution. Particles that did not interact in these detectors were identified by requiring consistency between the signals in the two Cherenkov detectors, as well as between the signals in the relatively thin ion chambers ($I2$ and $I4$) mounted before and after the Cherenkov detectors. To perform these consistency checks we began by making two-dimensional histograms of the signals from $C1$ versus $C2$ and from $I2$ versus $I4$. For each charge peak in these histograms, a mean and a standard deviation was determined. Smoothed curves at 3 s.d. from these charge peaks were then used to define different regions on each histogram. Signals found outside the regions bounded by these curves were then defined to be due to particles that had interacted in the detectors [10]. These procedures removed between 10% and 20% of the particles, consistent with the expected rates.

A correction was applied for those particles that were removed because they interacted in the Cherenkov detectors. This correction was calculated from a model describing the transport and interaction of particles through the detector array, and required assuming values of the total charge-changing cross sections in the materials of the detectors. The cross sections used in this transport calculation were taken from the best fit parametrization derived in Sec. IV C. Results from this transport calculation were compared, where possible, to the number of particles that interacted, and were found to be consistent.

Two additional selections were applied. One removed interactions that produced very small apparent charge changes near the beam peak. Its effect can be seen in the empty circle in Fig. 3. This selection removed less than 5% of the number of fragments with $\Delta Z = -1$. The second selection removed events whose signals in the ion chambers and Cherenkov detectors were more than 8 s.d. of the beam peak from the axis of the charge islands. In the worst case this selection removed less than 0.1% of all the events. Both selections improved the separation of the charge peaks.

An additional correction was made for interactions occurring near, but not in, the targets (in the air, etc.) by using the target-out runs. For each type of fragment, the number of events found in the target-out run, after the application of the above selections, was subtracted from the number in the target-in run, after scaling to the same number of incident projectiles. The effect of these corrections are included in the estimates of the systematic uncertainties.

IV. TOTAL CHARGE-CHANGING CROSS SECTIONS

A. Measurements

To compute the total cross sections requires a determination of the number of particles entering the target, N_0^T; the number of particles entering the empty target volume (target-out or "blank"), N_0^b; the number of beam particles that do not interact in the target, N_P^T, and the number of beam particles that do not interact in the empty target volume, N_P^b. In addition, it is necessary to know the number density n_T and thickness x_T of the target. The total charge-changing cross section is computed from [8]

$$\sigma(P,T) = \frac{1}{n_T x_T} \left\{ \ln\left(\frac{N_0^T}{N_P^T}\right) - \ln\left(\frac{N_P^b}{N_0^b}\right) \right\}. \tag{1}$$

This expression depends only on the ratio of the numbers for the target-in and target-out events.

To determine N_P^T and N_P^b, the number of incident particles that have not interacted, the beam peak and width are found by fitting a Gaussian distribution to the sum of the signals from ion chambers $I2$, $I3$, and $I4$. A similar fit is also applied to the distribution of the sum of the signals from Cherenkov detectors $C1$ and $C2$. An ellipse in I-C space is formed centered on the beam peak with axes of ± 3 s.d. in both the I and C directions. Events that fall within this ellipse are counted (N_P^T, N_P^b) and are defined to be noninteracting beam particles. This criterion is large enough to include essentially all the beam peak but small enough not to include events that have had a charge change. The deduced cross sections are almost independent of the beam selection criteria between 3 and 6 s.d., varying by less than 2%. The corrections to the total cross sections due to the target-out runs, which included corrections for interactions in the detectors, were typically in the range 19–24 %, consistent with the thickness of the detectors, and introduced the dominant factors in the final statistical uncertainties. The only identified sources of systematic uncertainties were in the choice of the 3 s.d. selection and the uncertainties in the target thicknesses. These were $\approx 10\%$ for the Li target, 1.2% for the Pb targets, and less than 1% for the remaining targets.

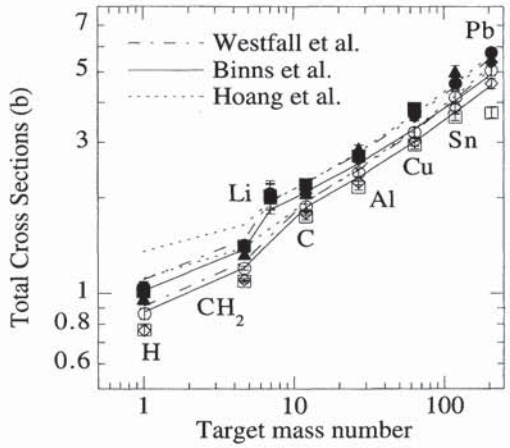

FIG. 4. Target dependence for the Kr and Ag beams of the total charge-changing cross section compared with that predicted by Binns *et al.* [2], Westfall *et al.* [13], and Hoang *et al.* [15]. The data points are (○) 1502*A* MeV Kr beam, (□) 1198*A* MeV Kr beam, (◇) 700*A* MeV Kr beam, (●) 1452*A* MeV Ag beam, (■) 1212*A* MeV Ag beam, (◆) 1001*A* MeV Ag beam, (▲) 504*A* MeV Ag beam. These same cross sections are also displayed in more detail in Figs. 7–11.

The hydrogen (H) cross sections were calculated using those derived from the polyethylene (CH_2) and carbon (C) targets from the relation

$$\sigma(P,\mathrm{H},E)=\tfrac{1}{2}[3\sigma(P,\mathrm{CH}_2,E)-\sigma(P,\mathrm{C},E)]. \quad (2)$$

The values of the total cross sections are listed in Table II, together with their statistical and systematic uncertainties. Consistent values could not be determined for the Ag runs at 612*A* MeV incident energy, since a bad beam focus during that run made the determination of N_P^T unreliable. A global view of the measured values of $\sigma(P,T,K)$ as a function of target mass in shown in Fig. 4, along with the predictions of some of the models to be described below.

These total charge-changing cross sections are also plotted in more detail in Figs. 7–11, below. They show the general features seen in many similar studies [2,12–16]. The major deviations from the general trends are the larger than expected cross sections in the Li target and the smaller than expected cross sections for the intermediate-energy Kr in Pb. The Li deviation is likely due to the one proton in an outer shell of the Li nucleus [17]. The energy dependence of these cross sections is discussed in Sec. IV D.

These measured total charge-changing cross sections can be compared with those predicted by different models. Abrasion-ablation models [18–20] have been formulated that provide acceptable fits to previously published measurements. However, when one of these models [18,19], was used in an attempt to predict our cross sections, which are obtained in a different charge region, the agreement was unsatisfactory (we have not yet been able to compare our results with the recently published model of Brohm and Schmidt [20]).

The transparency of nuclei has been modeled by Karol [21] in a determination of total interaction probabilities, but even after allowing for the difference between total interaction cross sections and total charge-changing cross sections, a comparison with the predictions of this model and our measurements results in reduced chi squared values χ_ν^2 much larger than those from a simple hard sphere model. In these theories the energy dependence of the cross sections is based on the energy dependence of the nucleon-nucleon cross sections or the energy-dependent mean free path of a nucleon in a nucleus.

An alternative approach, widely used in studies of cosmic ray propagation, is a semiempirical parametrization of measured data, such as that introduced and extensively modified by Silberberg and Tsao [22–24]. This model, which concentrates on hydrogen as a target, introduces a number of nonphysical discontinuities in the partial cross sections, but is generally capable of reproducing the measurements to within 35%. To achieve this level of agreement has required the introduction of a large number of parameters and special cases, and has resulted in a complex algorithm for computing the cross sections. These considerations led us to return to a study of simpler geometric models, seeking improvements sufficient to provide reasonable predictions, with a minimum of adjustable parameters.

B. Hard sphere models

The hard sphere model, first introduced in its simplest form by Bradt and Peters [12], gives a relatively accurate and simple representation of the total nucleus-nucleus cross sections. In this model the total cross section is that of a pair of hard spheres colliding with a small overlap:

$$\sigma(R_P,R_T)=\pi(R_P+R_T-\Delta R)^2, \quad (3)$$

where R_P and R_T, the projectile and target nuclear radii, are usually taken to be

$$R=r_0A^{1/3}, \quad (4)$$

with A being the mass number of the nucleus and where ΔR, the overlap parameter, is written as

$$\Delta R=r_0\delta, \quad (5)$$

with r_0 and δ as constants to be determined. Originally, values of $r_0=1.45$ fm and $\delta=1.17$ were found for cosmic ray nuclei between C and Fe interacting in a glass target [12]. A number of variations of the form of the overlap term and of the values of these constants have been proposed to achieve better fits to measured cross sections.

Using ^{56}Fe nuclei accelerated at the Bevalac to 1.88*A* GeV interacting in a wide range of targets from hydrogen to uranium, Westfall *et al.* [13] fitted their total charge-changing cross sections to Eq. (3) with $r_0=1.35\pm0.02$ fm, $\delta=0.83\pm0.12$, but found that for a hydrogen target it was necessary to use an effective mass $A_H^{\mathrm{eff}}=0.089$.

Binns *et al.* [2], using heavier projectiles of Kr, Xe, Ho, and Au having the maximum rigidity available from the Bevalac interacting in targets from hydrogen to aluminum, found it necessary to modify the overlap term:

$$\Delta R=r_0\delta(A_P+A_T)^{\varepsilon}, \quad (6)$$

TABLE III. New hard sphere parameters fitted to Eqs. (3) and (4) with overlap terms (5), (6), and (8) including the ten total nuclear charge-changing cross sections from Binns *et al.* [2] and the six from Geer *et al.* [26].

Overlap equation	r_0 (fm)	δ	ε	A_H^{eff}	χ^2_ν
(5)	1.361±0.010	1.07±0.06		0.065±0.008	6.22
(6)	1.39±0.04	0.88±0.15	0.066±0.068	0.082±0.009	6.37
(8)	1.278±0.005	4.9±0.3		0.156±0.013	6.15

with $\delta=0.209\pm0.003$ and $\varepsilon=1/3$, while keeping the values for $r_0=1.35$ fm and $A_H^{\text{eff}}=0.089$. They found that this form gave results consistent with the experimental results of Westfall *et al.* [13] for the lighter projectiles but a better representation for their heavier projectiles.

For Bevalac projectiles of carbon to nickel interacting in targets of hydrogen, helium, and carbon, Webber *et al.* [14] fit an overlap term of the form

$$\Delta R = r_0[\,\delta - \varepsilon A_T - b' A_P^{1/3} A_T^{1/3}], \tag{7}$$

with $r_0=1.35$ fm, $\delta=1.0074$, $\varepsilon=0.013$, and $b'=0.048$. The lack of symmetry of this form with respect to the projectile and target masses has led us not to consider it further here. However, a more detailed description of the application of this approach to the results for these heavy projectiles can be found in Nilsen [10].

Hoang *et al.* [15], using Glauber theory [25] and the cross sections measured by Westfall *et al.* [13], developed an overlap term, for large A, of the form

$$\Delta R = \frac{r_0 \delta}{(A_P^{1/3} + A_T^{1/3})}, \tag{8}$$

with $r_0=1.31\pm0.01$ fm and $\delta=4.45\pm0.15$. It should be noted that this overlap term decreases with increasing A, whereas those in Eqs. (6) and (7) increase and that in Eq. (5) is constant. With the exception of the model of Binns *et al.* [2], these models were derived from measurements made with lighter projectiles and/or light targets and may not fit the cross sections of the heavier nuclei considered here.

We have fit the cross sections measured in this work with new parameters in the hard sphere models, without regard to energy [Eqs. (3)–(8)] both with and without including ten additional Bevalac cross sections reported by Binns *et al.* [2] and six additional higher energy AGS 10.6A GeV Au projectile cross sections from Geer *et al.* [26]. These latter cross sections were corrected for electromagnetic dissociation, which is insignificant at Bevalac energies. New values for r_0 and the parameters associated with ΔR [Eqs. (5)–(8)] have been found, and some of the best fit results are given in Table III.[1]

None of these new fits to the Ag and Kr data were able to achieve χ^2_ν values less than ≈6.59. Lower χ^2_ν values resulted when the additional cross sections determined by Binns *et al.* [2] and Geer *et al.* [26] were included and are shown in Table III. This improvement was, most likely, related to the inclusion of more cross sections at the highest energies where the energy dependence of the cross sections appear to be less. These new fits are discussed in greater detail by Nilsen [9].

In none of the fits have any correlations between the different cross sections been taken into account. The large values of χ^2_ν are thought to be a result of the simplicity of the models to describe the physical details reflected in the cross sections and the rather small uncertainties of the cross section measurements.

C. Electron measured nuclear radii

A somewhat better fit to the total charge-changing cross sections was obtained by modifying the assumption that $R \propto A^{1/3}$ in Eq. (4). Nuclear charge radii R_e have been determined from electron scattering measurements [28,29]. Although these references do not give R_e for ^{84}Kr or ^{109}Ag, these can be estimated with some degree of confidence by interpolation. The values of R_e based on the equivalent uniform model [28] are shown in Fig. 5 as a function of the atomic mass and can be seen to be fit by a power law of the form $R \propto A^{0.281\pm0.003}$, which is significantly different from the $A^{1/3}$ commonly assumed.

A suggestion that the nuclear charge radii may be better suited for modeling charge-changing cross sections can be

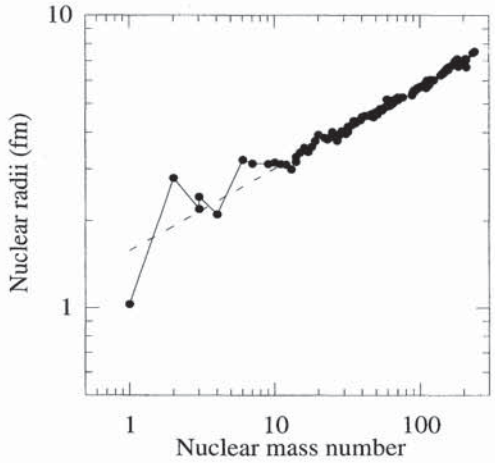

FIG. 5. Nuclear radii as a function of the mass number. These radii are taken from Collard *et al.* [28] and de Vries *et al.* [29]. The dotted line is a power-law fit $(1.58\pm0.02)A^{(0.281\pm0.003)}$.

[1]Values of $\sigma(P,T,K)$ for La at 1.2A GeV in H, C, and Pb have been reported by Christie *et al.* [27]. They have relatively large uncertainties, particularly for Pb, and have not been included in this analysis, but are consistent with the fits.

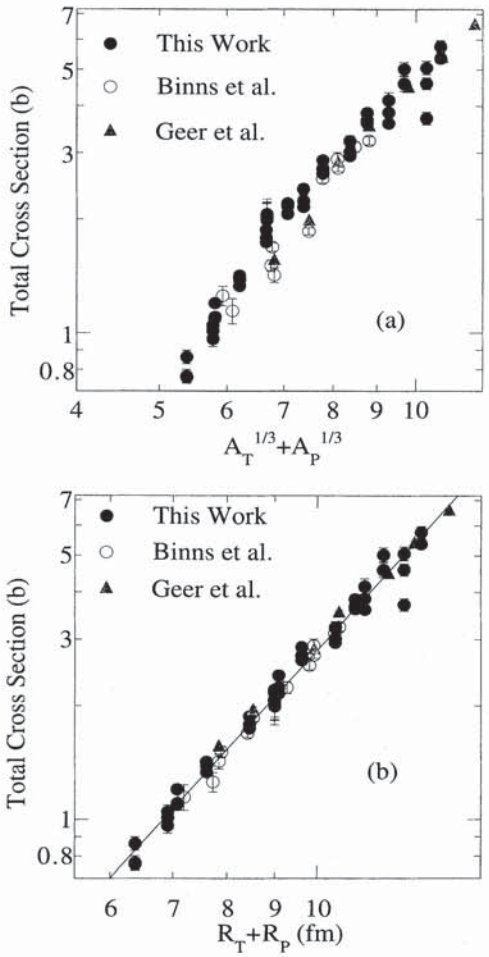

FIG. 6. (a) Total charge-changing cross sections plotted against $A_T^{1/3}+A_P^{1/3}$ for the beams of krypton and silver, together with the cross sections from Binns *et al.* [2] and Geer *et al.* [26] for beams of xenon, holmium, and gold, on all targets. (b) The same total charge-changing cross sections as in (a) plotted as a function of R_T+R_P. The line is a power-law fit to the cross sections of the form $[(5.40\pm0.14)\times10^{-3}](R_T+R_P)^{(2.717\pm0.012)}$.

TABLE IV. New hard sphere parameters using R_e fitting to Eq. (3) with overlap terms (5), (6), and (8).

Overlap equation	S	α	ε	χ^2_ν
(5)[a]	1.249±0.010	2.98±0.08		5.68
(5)[b]	1.277±0.006	3.20±0.05		5.59
(6)[a]	1.25±0.02	3.0±0.5	−0.004±0.041	5.82
(6)[b]	1.282±0.018	3.1±0.3	0.007±0.03	5.69
(8)[a]	1.08±0.005	13.6±0.4		5.63
(8)[b]	1.107±0.003	15.9±0.3		6.27

[a]There are 43 values of Kr and Ag $\sigma(P,T,K)$ used in these fits.
[b]These fits include the ten additional values of the total cross section from Binns *et al.* [2] and the six additional values from Geer *et al.* [26] with the electromagnetic contribution removed.

seen in Fig. 6. Here we have plotted the cross sections as a function of $A_T^{1/3}+A_P^{1/3}$ in Fig. 6(a) and as a function of the nuclear charge radii in Fig. 6(b). It is clear that using the nuclear charge radii reduces the fluctuations and that the results for the heaviest projectiles are brought into better accord with those for the lighter Kr and Ag. The cross sections have been fit to a power law in R_T+R_P, Fig. 6(b), which shows that the cross sections are much better ordered by R_e.

We therefore replaced the reliance on mass numbers in the hard sphere models with a dependence on R_e. In addition, a scaling factor S was introduced to generate nuclear, R_n, rather than electron, measured charge radii. Thus, in Eqs. (3)–(8), we replaced $r_0\delta$ by a new variable α and $r_0A^{1/3}$ by SR_e. A significant advantage of this approach is that when using R_e rather than A it is no longer necessary to treat hydrogen as an exception. The parameters of the hard sphere models with the smallest values of χ^2_ν are given in Table IV and the values of the parameters dependent on R_e, R_n, and the effective r_0, i.e., $R_e/A^{1/3}$, for all the nuclei used in the fits are given in Table V.

In spite of the improvements illustrated in Fig. 6(b), Table IV shows values of χ^2_ν that are only slightly better than those in Table III. In Equation (6) the parameter ε tends to assume small values thus reducing the overlap term to that of Eq. (5), which had the lowest χ^2_ν. The small values of ε suggest that

TABLE V. Values of R_e and the related parameters r_0(eff) and R_n based on the equivalent uniform model [28,29] and R_W, the nuclear radii used by Westfall *et al.* [13].

	H	Li	C	Al	Fe	Cu	Kr
$r_0(\text{eff})=R_e/A^{1/3}$ fm	1.034	1.64	1.36	1.25	1.27	1.28[a]	1.22[a]
$R_W=1.35A^{1/3}$ fm	1.35	2.57	3.09	4.05	5.16	5.39	5.91
R_e fm	1.034	3.13	3.11	3.75	4.85	5.11	5.34
$R_n=SR_e$ fm[b]	1.32	4.00	3.97	4.79	6.19	6.52	6.82
	Ag	Sn	Xe	La	Ho	Au	Pb
$r_0(\text{eff})=R_e/A^{1/3}$ fm	1.23[a]	1.20	1.21[a]	1.21[a]	1.22[a]	1.17	1.19
$R_W=1.35A^{1/3}$ fm	6.45	6.63	6.86	6.99	7.40	7.85	7.99
R_e fm	5.87	5.90	6.15	6.27	6.69	6.81	7.04
$R_n=SR_e$ fm[b]	7.39	7.53	7.85	8.01	8.54	8.70	8.99

[a]Values were estimated based on interpolation of the tabulated radii.
[b]Using the value of $S=1.277$ for the best fit found in Table IV.

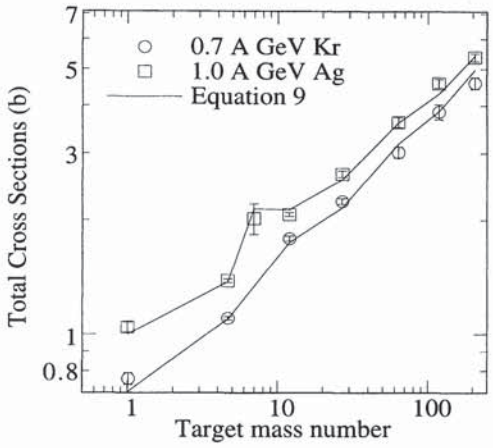

FIG. 7. Total charge-changing cross sections for $0.7A$ GeV krypton and $1.0A$ GeV silver beams on all targets. In order to guide the eye, lines connect the calculated values based on the overlap terms defined by Eq. (9) and the electron measured nuclear radii.

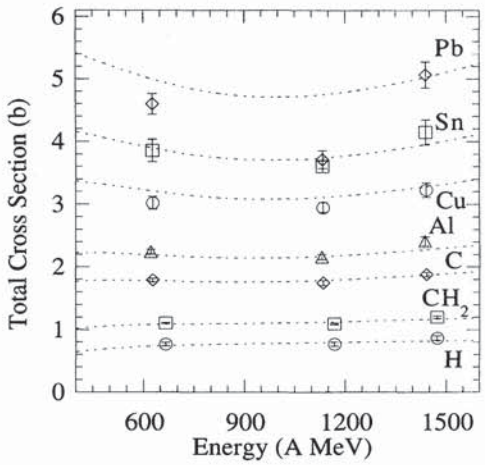

FIG. 8. Energy dependence of the total charge-changing cross sections for the krypton beam on all of the targets. The dotted lines are from Eq. (11).

the more elaborate overlap terms represent attempts to compensate for the irregularities in the sizes of the nuclei. The parameter $S=1.277$, found from the fit to Eq. (5), tends to be larger than expected physically and corresponds to a value for R_n of 6.19 fm for an iron nucleus; cf. the value R_W of 5.16 fm determined by Westfall *et al.* [13]. On the other hand, the value of $S=1.11$, found from Eq. (8), would correspond to a value of $R_n=5.38$ fm.

Equation (9) then represents our best fit form for the energy-independent cross sections:

$$\sigma(R_P,R_T)=\pi[R_P+R_T-(3.20\pm0.05)]^2, \tag{9}$$

where the values of R_P and R_T are taken from Table V. The total charge-changing cross sections for $700A$ MeV krypton and $1001A$ MeV silver beams are plotted in Fig. 7 as a function of target mass, along with Eq. (9). The large values of χ^2_ν found in the fitting procedures described in this section reflect the inadequacy of the models to describe the physical details reflected in the cross sections, at the rather small levels of uncertainty allowed by these measurements. Note that the process of fitting with these functions generate a correlation between the parameters S and α. A calculation of the root-mean-squared relative error shows that the fits are typically $<10\%$. This level of precision is adequate for most of the relevant astrophysical applications. Brohm *et al.* [30] have reported charge-changing cross sections for many isotopes, stable and unstable, of elements lighter than Kr. Although for most of these isotopes there are no measurements of the charge radii, in the few cases where Eq. (9) can be used we find reasonable agreement with the measured elemental cross sections.

D. Energy scaling of the total cross sections

These models all assume that the cross sections do not depend on energy. However, our measured cross sections show significant changes in $\sigma(P,T,K)$ with energy. Examples of these changes are given in Figs. 8–11. It can be seen that for both projectiles there are small but significant variations with energy which increase with increasing mass of the targets. Even a light target such as CH_2, where the values of $\sigma(P,CH_2,K)$ have the smallest experimental uncertainties, show variations with energy (Figs. 8 and 10) that are statistically significant. These variations of the total cross sections with energy are different for the two beams and there is no obvious way to predict how they will vary at higher energies.

We have attempted to allow for the energy dependence by modifying Eq. (3) to include logarithmically energy dependent scaling factors $F(E)$ and $G(E)$, as shown in Eq. (10):

$$\sigma(R_P,R_T,E)=\pi F(E)[R_P+R_T-G(E)\Delta R]^2,$$
$$F(E)=1+F_1\ \ln(E)+F_2[\ln(E)]^2,$$
$$G(E)=1+G_1\ \ln(E)+G_2[\ln(E)]^2. \tag{10}$$

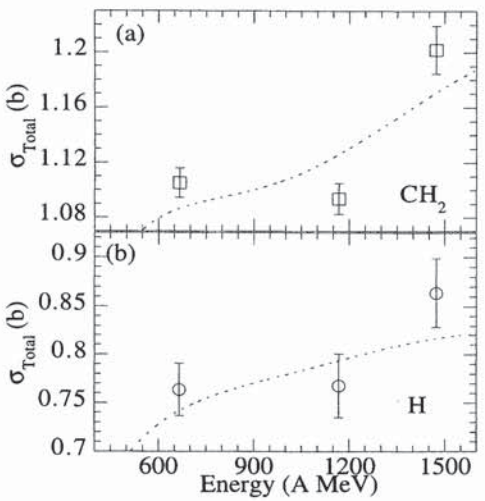

FIG. 9. Total charge-changing cross sections for a krypton beam on a polyethylene target (a) and the deduced cross section for a hydrogen target (b) as a function of the energy. The dotted lines are from Eq. (11).

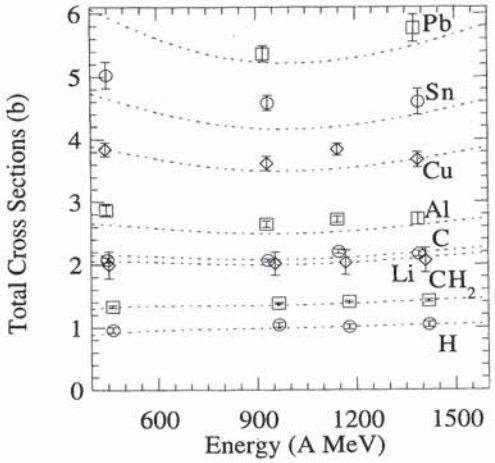

FIG. 10. Energy dependence of the total charge-changing cross sections for the silver beam on all of the targets. The dotted lines are from Eq. (11).

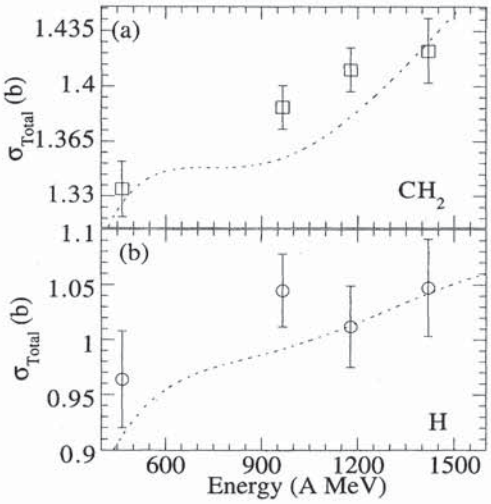

FIG. 11. Total charge-changing cross sections for a silver beam on a polyethylene target (a) and the deduced cross section for a hydrogen target (b) as a function of energy. The dotted lines are from Eq. (11).

Here ΔR is of the same form used earlier and E is the total energy $(K+m_0c^2)$ per nucleon. This logarithmic expression of energy scaling is inspired by that used at higher energies by the Particle Data Group [31] to parametrize proton-proton and proton-neutron total cross sections. From limiting fragmentation arguments, the total cross sections, excluding electromagnetic effects, are expected to be energy independent apart from logarithmic corrections [32]. The resulting values of the various parameters in Eqs. (5) and (8), after including energy scaling, are given in Table VI.

The resulting fits, shown in Figs. 8–11, have only slightly smaller χ^2_ν values than those found without energy scaling. The best fit is provided by (5)[b], but the figures show that the resulting Eq. (11) still does not fully reproduce the behavior of the measured values of $\sigma(P,T,K)$:

$$R_n=(1.80\pm0.09)R_e,$$

$$\sigma(R_P,R_T,E)=\pi F(E)[R_P+R_T-(8.9\pm1.4)G(E)]^2, \tag{11}$$

$$F(E_T)=1-(1.61\pm0.16)\ln(E)+(1.18\pm0.14)[\ln(E)]^2,$$

$$G(E_T)=1-(1.51\pm0.20)\ln(E)+(1.04\pm0.18)[\ln(E)]^2.$$

Including the higher energy, $10.6A$ GeV, cross sections of Geer *et al.* [26], case (5)[c], yields greatly different parameters and increases χ^2_ν. This suggests that Eq. (11) cannot be reliably extrapolated to much higher energies than those studied directly in this work.

Here again, as was the situation when the cross sections were assumed to be independent of energy, the values of S for the best fits are larger than might be expected physically, $S=1.80\pm0.09$, which is the value needed to fit case (5)[b] (Table VI), would imply a value of R_n of 8.76 fm for an iron nucleus. This R_n is much larger than that of 5.16 fm found by Westfall *et al.* [13]. The large value of R_n is partially compensated by the value of $F[E=(1.88+0.93)A$ GeV$]=0.596$, giving an effective $R_n=5.22$, but clearly this factor will not help as much for lower energy interactions.

V. PARTIAL CHARGE-CHANGING CROSS SECTIONS

The partial charge-changing cross sections were determined only where there were cleanly separated peaks in the

TABLE VI. Fit parameters for hard sphere models with overlap terms (5) and (8) using R_e, energy scaling, and energy scaling of the overlap term.

Equation	S	α	F_1	F_2	G_1	G_2	χ^2_ν
(5)[a]	1.75±0.03	8.2±0.4	−1.512±0.012	1.11±0.04	−1.41±0.04	0.96±0.06	4.65
(5)[b]	1.80±0.09	8.9±1.4	−1.61±0.16	1.18±0.14	−1.51±0.19	1.04±0.18	3.92
(5)[c]	1.34±0.04	4.0±0.4	−0.28±0.10	0.09±0.03	−0.40±0.10	0.11±0.04	4.88
(8)[a]	1.37±0.06	47±11	−1.24±0.19	0.95±0.16	−1.6±0.3	1.1±0.2	4.73
(8)[b]	1.38±0.06	49±11	−1.28±0.18	0.98±0.14	−1.6±0.3	1.1±0.2	4.07
(8)[c]	1.14±0.02	21±3	−0.23±0.07	0.09±0.02	−0.60±0.11	0.21±0.04	4.86

[a]There are 43 values of Kr and Ag $\sigma(P,T,K)$ used in these fits.

[b]These fits include the ten additional values of $\sigma(P,T,K)$ from Binns *et al.* [2].

[c]These fits include the six additional values, at $10.6A$ GeV, from Geer *et al.* [26] with the electromagnetic contribution removed.

charge distributions with peak to valley ratios >2.0, so that the number of particles in each peak was a direct measure of the partial cross sections. A measured pseudocharge distribution is shown in Fig. 3 (see Sec. III). Superimposed on this distribution are Gaussians with peaks and widths fitted to the data.

With thick targets a correction must be made for multiple interactions. This correction was made by calculating the propagation of particles through the target and predicting the number of particles of each charge that should have been measured [10]. In this calculation the target is treated as 100 slabs, each 0.2% or less of an interaction length. The predicted numbers are then compared to the measurements. The initially assumed values of the partial cross sections, which were based on the raw numbers observed, are then adjusted until the weighted squared differences between the numbers calculated and counted in the pseudocharge peaks are minimized [33]. This thick target correction has been discussed in more detail by Geer *et al.* [26].

The total cross sections used in the propagation were calculated from Eq. (9), except for the special cases of the beam and its two neighboring charges, where the actual measured cross sections for the beam were used. The required partial cross sections were calculated using the parametric representation of Cummings *et al.* [7], except for interactions resulting in fragments with $Z_P=\pm 1$, for which the uncorrected measured values of the partial cross sections were adopted. A check for the dependence of the deduced final values of the partial cross sections on those calculated from the parametric representation was performed by changing the values of these cross sections by 10%. The resulting values of the deduced cross sections corrected for the thick target varied only slightly. For example, the final values of the $1212A$ MeV Ag cross sections on a Cu target are changed in such a case by at most 1.2%, showing that this correction procedure is quite insensitive to the assumed values of the cross sections.

Some of these resulting cross sections are shown in Fig. 12, together with the total associated uncertainties. Also shown in these figures are comparisons with predictions based on various models. A complete list of the 1419 values of $\sigma_{\Delta Z}(P,T,K,\Delta Z)$ measured in this study and similar plots for all of the data are given in Ref. [10]. Also shown there are the statistical and systematic uncertainties that can be assigned to these values.

A. Power-law representation

The simplest representation of the behavior of the partial cross sections is to assume that they follow a power law in ΔZ. Such a relationship has been seen in many other experiments [2,7]. However, the largest and smallest charge changes generally do not follow such a simple relationship. In addition, in specific cases even the intermediate charge changes can deviate from such simple behavior because of the physics of the nuclear structure involved in forming a relatively stable nucleus; e.g., the fragments of Fe nuclei show a noticeable odd-even effect [6].

The nonhydrogen values of $\sigma_{\Delta Z}(P,T,\Delta Z)$ for fragments with $-20\leq\Delta Z\leq -2$, along with those reported by Binns *et al.* [2] and Cummings *et al.* [7], have been fit to power laws of the form $\sigma_\epsilon|\Delta Z|^{-\epsilon}$. A histogram of the values of χ^2_ν for each set of cross sections, shown in Fig. 13, confirm the universality of the power-law fits. The two runs with the largest χ^2_ν are $556A$ MeV Ag on Pb and $449A$ MeV Ag on C, respectively (energies are in the center of the target), which are two of the lowest energy runs studied. The energy dependence of the exponent $-\epsilon$ and scaling parameter σ_ϵ from the power-law fits to the particular case of Kr in C cross sections are shown in Fig. 14. The fact that the hydrogen cross sections $\sigma_{\Delta Z}(P,H,\Delta Z)$ do not follow a power law, but instead decrease more rapidly than expected as ΔZ increases, suggests that for such a small target nucleus at these low Bevalac energies the modes of fragmentation are different than those induced by heavier target nuclei. It is of interest to note that for much higher energy projectiles, Geer *et al.* [26] find a power-law behavior for the partial cross sections of $10.6A$ GeV Au in a hydrogen target unlike the exponential dependence found at lower energies [7].

A Li target, the lightest nonhydrogen target that can be easily handled, was included to allow a comparison of the Li cross sections with the hydrogen cross sections. It is clear, from Figs. 12(b) and 12(c), that these cross sections follow a power law similar to those for the heavier targets, and thus it appears that the behavior of the cross sections in hydrogen targets is different from those in any of the other targets we have studied.

B. Partial charge-changing cross section models

Cummings *et al.* [7], using heavier projectiles than those studied here, parametrized their global power-law expression for nonhydrogen targets as

$$\sigma_{\Delta Z}(A_P,A_T,K,\Delta Z)=p_1(A_P^{1/3}+A_T^{1/3}-p_2)\left(1-\frac{K}{p_3}\right)|\Delta Z|^{-[p_4(1+A_P/p_5)(1+A_T/p_6)(1-K/p_7)]} \tag{12}$$

and for a hydrogen target as

$$\sigma_{\Delta Z}(A_P,H,K,\Delta Z)=q_1A_P^{q_2}\left(\frac{K}{E_1}\right)^{q_3}\times\begin{cases}\exp\left\{-\left[\dfrac{|\Delta Z|}{q_4}\left(\dfrac{K}{E_1}\right)^{-q_5}\right]\right\}, & |\Delta Z|\leq q_6,\\ \exp\left\{-\left[\left(\dfrac{q_6}{q_4}+\dfrac{(|\Delta Z|-q_6)}{q_7}\right)\left(\dfrac{K}{E_1}\right)^{-q_5}\right]\right\}, & |\Delta Z|>q_6\end{cases} \tag{13}$$

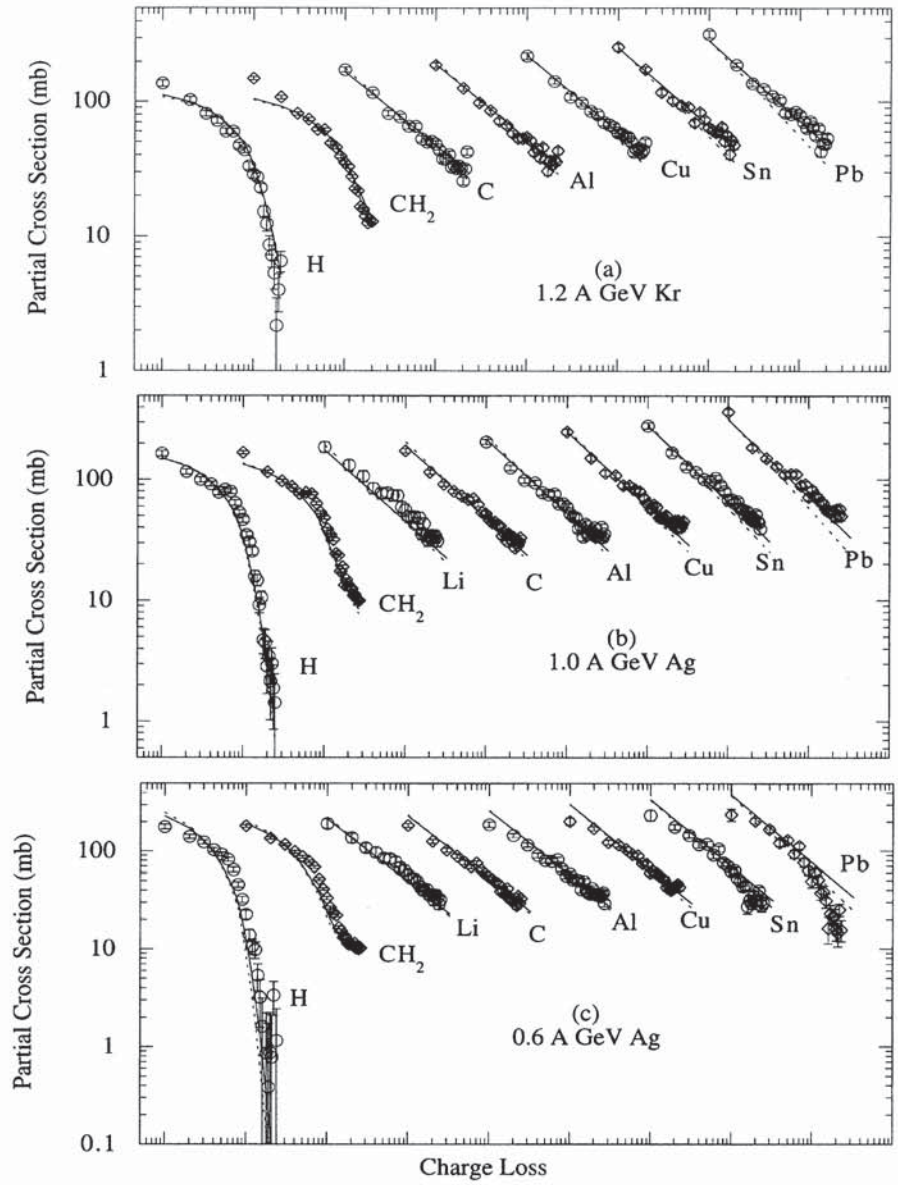

FIG. 12. (a) Partial charge-changing cross sections between $\Delta Z=-1$ and about -20 for the $1.2A$ GeV krypton beam on all targets. (b) The same for the $1.0A$ GeV silver beam. (c) The same for the $0.6A$ GeV silver beam. The solid lines are those from the new fit to Eqs. (13) and (14) and the dotted lines are those predicted by the expressions of Cummings *et al.* [7]. The different targets are separated by factors of 10 in ΔZ, charge loss, and for each target the largest value of the cross section is for $\Delta Z=-1$.

These parametrizations were only applied to charge changes $-2\geq\Delta Z\geq-20$. The parameters found are listed in Table VII. These expressions for $\sigma_{\Delta Z}(P,T,K,\Delta Z)$ diverged at high energy rather than reaching a limiting value.

Examples of the comparison between our new measurements and these predictions are shown in Fig. 12. It can be seen that the measurements deviate significantly from the predictions, particularly for the heaviest targets. The curves representing the predictions have been extended to cover the full range of ΔZ to show how the $\Delta Z=-1$ and $\Delta Z<-20$ values of $\sigma_{\Delta Z}(P,T,K,\Delta Z)$ deviate from those used for the fits.

The values of $\sigma_{\Delta Z}(P,T,K,\Delta Z)$ measured here, together with those of Binns *et al.* [2] and Cummings *et al.* [7], have been used to reevaluate the parameters of Eqs. (12) and (13). Including the values of $\sigma_{\Delta Z}(P,T,K,\Delta Z)$ obtained at $10.6A$ GeV by Geer *et al.* [26] makes it difficult to evaluate Eqs. (12) and (13) with parameters that are acceptable for the lower energy cross sections, and hence they have been excluded from this analysis. These new parameters are compared with the original values in Table VII. Here N is the number of values of $\sigma_{\Delta Z}(P,T,K,\Delta Z)$ used in the fits.

Inclusion of the results of the present work in these fits increased the values of χ^2_ν significantly. In both cases some of the parameters have changed significantly. In Eq. (12) the parameter p_2 has dropped to a value consistent with zero and p_6 has increased by a factor of 10, lessening the dependence on the target mass.

We have not been able to improve the fit to the partial charge-changing cross sections in hydrogen. We have, however, derived a new form for the nonhydrogen parametric power-law model that yields slightly improved values for χ^2_ν and does lead to limiting fragmentation at high energies. This new model, which is a modification of the successful parametrization for heavy projectile nuclei by Cummings *et al.* [7], is designed to be energy independent at higher energies and

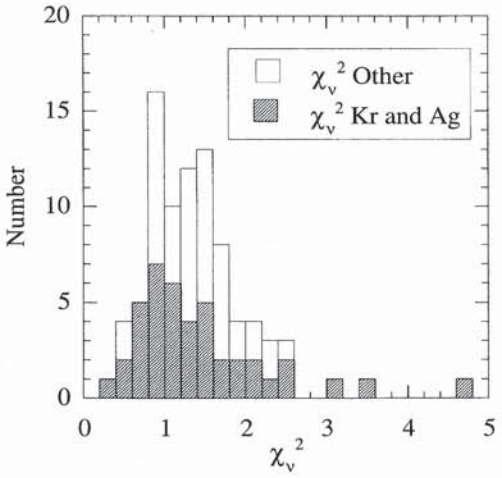

FIG. 13. Histogram of values of χ_ν^2 for power-law fits to the charge-changing cross sections, for nonhydrogen targets, for charge losses between $-2 \geq \Delta Z \geq -20$. "Other" refers to the cross sections of Geer *et al.* [26], Cummings *et al.* [6], and Binns *et al.* [2] excluding the iron beam data.

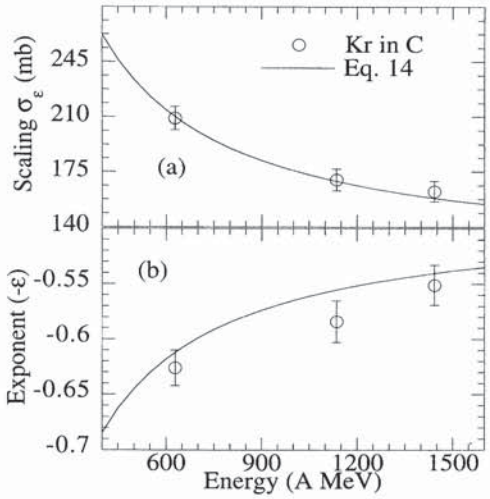

FIG. 14. Scaling parameter σ_ε and exponent $-\varepsilon$ from the power-law fits for Kr in C as a function of energy. The lines shows the predictions from Eq. (14).

still reproduce the cross sections. It is given in Eq. (14) and is applicable to the fragmentation of heavy beams on nonhydrogen targets for energies between $0.4A$ and $10.6A$ GeV. The exponent $-\epsilon$ and scaling parameter σ_ϵ predicted by Eq. (14) are shown in Fig. 14, where they are compared with the data:

$$\sigma_{\Delta Z}(A_P, A_T, K, \Delta Z) = p_1 (A_P^{1/3} + A_T^{1/3} - p_2) \left(1 + \frac{p_3}{K}\right) |\Delta Z|^{-p_4 [1 + A_P^{1/3}/p_5 + A_T^{1/3}/p_6 + p_7/K]}, \tag{14}$$

with the parameters given in Table VIII and a χ_ν^2 which is a little better than that of the earlier parametric fits (Table VII). Equation (14) may be somewhat more physically reasonable if these partial cross sections should become energy independent as limiting fragmentation would suggest. This new form should extrapolate better to higher energies than did Eq. (12), since it also adequately represents the $10.6A$ GeV cross sections. At high energies both the exponent and the scaling parameter become independent of the energy.

The large value of χ_ν^2 found in the fitting procedure described in this section reflect the inability of this simple model to fully describe the physical details reflected in the cross sections, at the rather small levels of uncertainty allowed by these measurements. It should also be noted that the model is not based on orthogonal functions and has a significant degree of correlation between many of its parameters. A consequence of this correlation is that individual parameters may change noticeably when the data points are

TABLE VII. New and old parameters for Cummings *et al.* [7] $E_1 \equiv 1.0A$ GeV.

	Hydrogen parameters [Eq. (13)]			Non-hydrogen parameters [Eq. (12)]	
	Old	New		Old	New
q_1	15.53±1.9 mb	18.0±1.1 mb	p_1	45±2 mb	37.0±0.8 mb
q_2	0.51±0.03	0.477±0.012	p_2	0.81±0.4	0.12±0.18
q_3	−1.28±0.03	−1.09±0.02	p_3	(3.48±0.16)A GeV	(4.76±0.15)A GeV
q_4	6.87±0.11	6.89±0.08	p_4	0.614±0.013	0.554±0.007
q_5	1.43±0.03	1.25±0.02	p_5	789±59	505±17
q_6	7.91±0.16	8.27±0.14	p_6	1173±204	(10±5)×10^3
q_7	4.15±0.07	4.41±0.06	p_7	(11.1±1.7)A GeV	(11.7±0.9)A GeV
χ_ν^2	2.07	4.29	χ_ν^2	1.81	3.10
N	303	438	N	795	1646

only slightly modified. This correlation implies a risk in using the fit to extrapolate into parameter spaces not well covered by the measurements. On the other hand, a calculation of the root-mean-square relative errors shows that the fits are typically $<15\%$.

Attempting more sophisticated parametrizations involving the nuclear charge radii and/or the average nucleus-nucleus total cross sections did not make any improvement and the added complications were not justified. In both Eqs. (12) and (14) there is a term $A_P^{1/3}+A_T^{1/3}-p_2$ that resembles the square root of the hard sphere expression for the total cross sections $\sigma(P,T)$. Replacing this term by the square root of the measured values of $\sigma(P,T,K)$ leads to a very poor fit to $\sigma_{\Delta Z}(P,T,K,\Delta Z)$. This poor fit presumably is a reflection of the fact that the values of $\sigma(P,T,K)$ are strongly dependent on charge changes other than those between -2 through -20, since the fractions of the partial charge-changing cross sections from $\Delta Z=-2$ to -20 of the total cross sections $\sigma(P,T,K)$ range from only 28.6% in lead to 86.2% in hydrogen.

C. Limiting fragmentation

At high enough energies, above reaction thresholds and resonances, it is expected that any fragmentation reaction would become energy independent except for corrections involving powers of $\ln(E)$ [32,34]. As the energy increases, the extra energy creates more particles or breaks up more of the subfragments instead of opening up new channels for the production of a given fragment or new particles.

Typical examples of the variations with energy for the partial cross sections for small ΔZ are shown in Fig. 15. In this figure the sum of small charge losses, $\Delta Z=-2$ to -6, is plotted for several projectiles in polyethylene targets. This summation was used to reduce the statistical uncertainties. The krypton, and possibly the silver, values could suggest that these cross sections are approaching a limit, but recent data by Geer *et al.* [26] show that for much heavier projectiles such as gold the sums of small charge-changing cross sections changed by nearly a factor of 2 between $\approx 1.0A$ and $10.6A$ GeV and the limiting value has certainly not been reached at Bevalac energies for such heavy nuclei. Measurements at intermediate energies are needed to establish the energy at which limiting fragmentation begins, although it appears likely that it is dependent on A_P.

TABLE VIII. Parameters for Eq. (14).

p_1	21.2±0.5 mb
p_2	1.08±0.15
p_3	(0.485±0.014)A GeV
p_4	0.094±0.013
p_5	1.11±0.02
p_6	10.8±1.6
p_7	(0.85±0.03)A GeV
χ_ν^2	2.84
N	1741

VI. CONCLUSIONS

The total charge-changing cross sections for krypton and silver nuclei in the energy range (450–1500)A MeV interacting in targets ranging in mass from hydrogen to lead have been measured and new parametrizations to organize these data have been produced. The simple $r_0A^{1/3}$ representation of the nuclear radii is inadequate to organize the values of $\sigma(P,T,K)$. The nuclear radii scaled from the charge radii measured by electron scattering give a better representation. Using electron measured radii has the advantage that there is no need to introduce a physically unrealistic effective hydrogen mass to incorporate cross sections on hydrogen targets into hard sphere models. It has also been shown that, in the hard sphere models, the more elaborate overlap terms, Eqs. (6)–(8), appeared to be compensating for the variations in nuclear size and did not represent any other physical processes. New parametrizations of the total cross sections have been introduced using the electron measured radii. Both energy-independent, Eq. (9), and energy-dependent, Eq. (11), parametrizations of $\sigma(P,T,K)$ have been introduced. The energy-dependent cross section formula is only expected to be valid over the energy range (500–1500)A MeV and should not be extrapolated.

The partial cross sections for fragment production, $\sigma_{\Delta Z}(P,T,K,\Delta Z)$, on all the targets heavier than hydrogen that we have studied follow power laws in the charge loss over a relatively wide range of ΔZ. The energy dependence of the large impact parameter cross sections, those with small values of ΔZ, shows evidence that limiting fragmentation has not been reached at the Bevalac energies. Partial cross sections for fragment production in hydrogen have a different dependence on the charge loss than those for any heavier targets, even one as light as lithium. The different functional form of the hydrogen partial cross sections suggests that the fragment charge dependence of $\sigma_{\Delta Z}(P,H,K,\Delta Z)$ could be dominated by the single-particle nature of the hydrogen nucleus.

New parameters have been found to describe the fragmen-

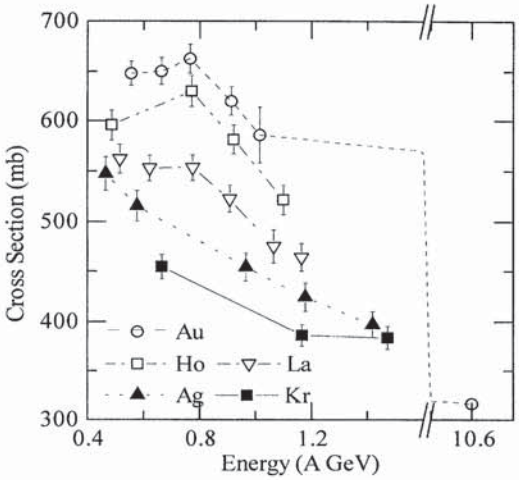

FIG. 15. Energy dependence of the sum of the charge-changing cross sections for $-2\geq\Delta Z\geq-6$ for beams of krypton, silver, lanthanum, holmium, and gold on a polyethylene target. The high energy gold value is shown with the correct slope, but a broken scale.

tation of ultraheavy nuclei on hydrogen targets. The form is unchanged from that found by Cummings *et al.* [7], Eq. (13). For targets heavier than hydrogen, a new partial charge-changing cross section form has been introduced [Eq. (14)] and fit to cross section data in the energy range (500–1500)A MeV on beams from iron to gold and targets from lithium to lead. This new parametrization is consistent with limiting fragmentation unlike our previous version which diverged at high energies.

ACKNOWLEDGMENTS

We are grateful to all those who assisted in this experiment. In particular, we thank W. R. Binns, E. C. Stone, B. W. Gauld, and L. Y. Geer for their assistance. We are indebted to the staff of the LBL Bevalac facility, especially H. J. Crawford, J. Engelage, L. Greiner, and M. Flores for their assistance. This work was funded in part by NASA grants.

[1] R. R. Clinton and C. J. Waddington, Astrophys. J. **403**, 644 (1993).
[2] W. R. Binns, T. L. Garrard, M. H. Israel, M. P. Kertzmann, J. Klarmann, E. C. Stone, and C. J. Waddington, Phys. Rev. C **36**, 1870 (1987).
[3] N. R. Brewster, Ph.D. thesis, University of Minnesota, 1984.
[4] W. R. Binns, J. R. Cummings, T. L. Garrard, M. H. Israel, J. Klarmann, E. C. Stone, and C. J. Waddington, Phys. Rev. C **39**, 1785 (1989).
[5] J. R. Cummings, Ph.D. thesis, University of Minnesota, 1989.
[6] J. R. Cummings, W. R. Binns, T. L. Garrard, M. H. Israel, J. Klarmann, E. C. Stone, and C. J. Waddington, Phys. Rev. C **42**, 2508 (1990).
[7] J. R. Cummings, W. R. Binns, T. L. Garrard, M. H. Israel, J. Klarmann, E. C. Stone, and C. J. Waddington, Phys. Rev. C **42**, 2530 (1990).
[8] M. P. Kertzmann, Ph.D. thesis, University of Minnesota, 1986.
[9] B. S. Nilsen, C. J. Waddington, W. R. Binns, J. R. Cummings, T. L. Garrard, L. Y. Geer, and J. Klarmann, Phys. Rev. C **50**, 1065 (1994).
[10] B. S. Nilsen, Ph.D. thesis, University of Minnesota, 1994.
[11] C. J. Waddington, Int. J. Mod. Phys. E **4**, 739 (1993).
[12] H. L. Bradt and B. Peters, Phys. Rev. **77**, 54 (1950).
[13] G. D. Westfall, L. W. Wilson, P. J. Lindstrom, H. J. Crawford, D. E. Greiner, and H. H. Heckman, Phys. Rev. C **19**, 1309 (1979).
[14] W. R. Webber, J. C. Kish, and D. A. Schrier, Phys. Rev. C **41**, 520 (1990).
[15] T. F. Hoang, B. Cork, and H. J. Crawford, Z. Phys. C **29**, 611 (1985).
[16] H. H. Heckman, D. E. Griner, P. J. Lindstom, and H. Shwe, Phys. Rev. C **17**, 1735 (1978).
[17] H. A. Enge, *Introduction to Nuclear Physics* (Addison-Wesley, Reading, MA, 1966).
[18] L. W. Townsend, J. W. Wilson, R. K. Tripathi, J. W. Norbury, F. F. Badavi, and F. Khan, NASA Technical Report No. 3310, 1993.
[19] F. F. Badavi, L. W. Townsend, J. W. Wilson, and J. W. Norbury, Comput. Phys. Commun. **47**, 281 (1987).
[20] T. Brohm and K.-H. Schmidt, Nucl. Phys. **A569**, 821 (1994).
[21] P. J. Karol, Phys. Rev. C **11**, 1203 (1975).
[22] R. Silberberg and C. H. Tsao, Phys. Rep. **191**, 351 (1990).
[23] L. Sihver, C. H. Tsao, R. Silberberg, T. Kanai, and A. F. Barghouty, Phys. Rev. C **47**, 1225 (1993).
[24] C. H. Tsao, R. Silberberg, A. F. Barghouty, L. Sihver, and T. Kanai, Phys. Rev. C **47**, 1257 (1993).
[25] R. J. Glauber, in *Lectures in Theoretical Physics*, edited by W. E. Brittin and L. G. Dunham (Interscience, University of Colorado, Boulder, 1958), Vol. 1, pp. 315–413.
[26] L. Y. Geer, J. Klarmann, B. S. Nilsen, C. J. Waddington, W. R. Binns, J. R. Cummings, and T. L. Garrard, Phys. Rev. C **51**, 334 (1995); L. Y. Geer, Ph.D. thesis, Washington University, 1995.
[27] W. B. Christie, J. L. Romero, F. P. Brady, C. E. Tull, G. P. Grim, B. McEachern, J. C. Young, H. J. Crawford, D. E. Greiner, P. J. Lindstrom, H. Sann, and U. Lynen, Phys. Rev. C **48**, 2973 (1993).
[28] H. R. Collard, L. R. B. Elton, and R. Hofstadter, in *Nuclear Physics and Technology*, edited by H. Schopper, Landolt-Börnstein, New Series, Group 1, Vol. 2 (Springer-Verlag, Berlin, 1967), p. 30.
[29] H. de Vries, C. W. de Japer, and C. de Vries, At. Data Nucl. Data Tables **36**, 495 (1987).
[30] T. Brohm *et al.*, Nucl. Phys. **A585**, 565 (1995).
[31] Particle Data Group, K. Hikasa *et al.*, Phys. Rev. D **45**, S1 (1992), III.83–III.90.
[32] J. Benecke, T. T. Chou, C. N. Uang, and E. Yen, Phys. Rev. **188**, 2159 (1969).
[33] F. James and M. Roos, Cern Program Library entry No. D506, 1989.
[34] H. Bøggild and T. Ferbel, Annu. Rev. Nucl. Sci. **24**, 451 (1974).

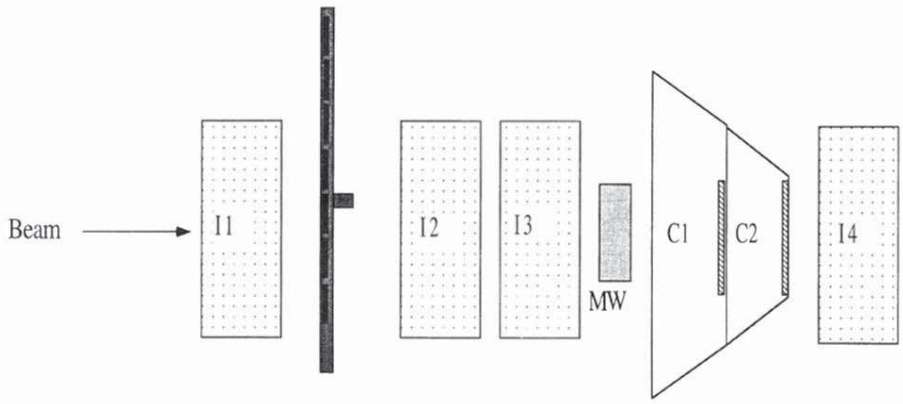

FIG. 1. HEAO Bevalac detector set up showing the relative position of the detectors used in this analysis. $I1$, $I2$, $I3$, and $I4$ are ion chambers. $C1$ and $C2$ are Cherenkov detectors. MW is a multiwire proportional chamber. The target changer is placed between $I1$ and $I2$. The array is 2.3 m long.